Proceedings of the ASME 2011 Conference on Smart Materials, Adaptive Structures and Intelligent Systems
SMASIS2011
September 18-21, 2011, Scottsdale, Arizona, USA

SMASIS2011-5219

ACTIVE DETECTION OF STRUCTURAL DAMAGE IN ALUMINUM ALLOY USING MAGNETO-ELASTIC ACTIVE SENSORS (MEAS)

David Conrad and Andrei Zagrai

New Mexico Institute of Mining and Technology,
Department of Mechanical Engineering
801 Leroy Pl., Socorro, New Mexico, 87801 USA

ABSTRACT

Many structural damage detection methods utilize piezoelectric sensors. While these sensors are efficient in supporting many structural health monitoring (SHM) methodologies, there are a few key disadvantages limiting their use. The disadvantages include the brittle nature of piezoceramics and their dependence of diagnostic results on the quality of the adhesive used in bonding the sensors. One viable alternative is the utilization of Magneto-Elastic Active Sensors (MEAS). Instead of mechanically creating elastic waves, MEAS induce eddy currents in the host structure which, along with an applied magnetic field, generate mechanical waves via the Lorentz force interaction. Since elastic waves are generated electromagnetically, MEAS do not require direct bonding to the host structure and its elements are not as fragile as PWAS.

This work explores the capability of MEAS to detect damage in aluminum alloy. In particular, methodologies of detecting fatigue cracks in thin plates were explored. Specimens consisted of two identical aluminum plates featuring a machined slot to create a stress riser for crack formation. One specimen was subjected to cyclic fatigue load. MEAS were used to transmit elastic waves of different characteristics in order to explore several SHM methodologies. Experiments have shown that the introduction of fatigue cracks created measurable amplitude changes in the waves passing through the fatigued region of the aluminum plate. The phase indicated sensitivity to load conditions, but manifestation in the cracked region lacked stability. Nonlinear effects were studied using plate thickness resonance, which revealed birefringence due to local stresses at the site of the fatigue crack. The resonance spectrum has also shown a frequency decrease apparently due to stiffness loss. Preliminary results suggest opportunities for fatigue damage detection using MEAS. Application of MEAS for the diagnosis of complex structures is currently being investigated.

INTRODUCTION

Modern structural health monitoring (SHM) increasingly relies on a diverse suite of sensing technologies. Piezoelectric transducers are widely using in SHM because of their high efficiency; however, limitations that can affect their application include the brittle nature of piezoelectric material as well as their dependence on the quality of an adhesive bond layer [1]. It is desirable to improve survivability of SHM sensors and eliminate, if possible, dependence of monitoring results on the quality of a bond layer between the sensors and the structure. Magneto-elastic active sensors (MEAS) [2] offer an alternative to piezoelectric transducers in applications where direct bonding to the structure is not desired, bond quality is a concern, or where a more mechanically robust sensor would be required.

MEAS utilize an effect of electromagnetic generation and reception of ultrasonic waves in conductive materials [3] and hence operate on the same principle as electromagnetic acoustic transducers (EMATs). However, in contrast to bulky and heavy EMATs, MEAS design is optimized and miniaturized for potentially embeddable applications and currently features sensors with diameters as small as ½ inch [4]. MEAS require two components; a wire coil and a stationary magnetic field. A time varying current is passed through the coil adjacent to a conductive host structure generating eddy currents. In nonferrous materials these eddy currents combined with a stationary magnetic field penetrating the material allows the generation of elastic waves through the Lorentz-force interaction [5]. MEAS also act as sensors where an elastic wave passing through a stationary magnetic field will induce current flow in the sensor coils. The primary advantages of MEAS are, first, the non-contact (or through paint) nature of their operation which allows performance independent of the integrity of the bond. Even though the bond layer does not impact sensor performance increasing liftoff results in decreased efficiency

[6]. Second, MEAS do not require brittle ceramics and can be manufactured to withstand demanding environments.

PRIOR WORK ON MEAS FOR DAMGE DETECTION APPLICATIONS

While SHM is a mature field, MEAS are relatively new and are not readily available. Little work has been done exploring the use of MEAS as a suitable alternative to piezoelectric transducers. Two methods have been demonstrated using MEAS for damage detection. It was shown that MEAS enables the Magneto-Mechanical Impedance (MMI) technique to detect changes in structural dynamic (vibration) signatures caused by damage [7]. This method employs a single sensor using continuous wave (CW) excitation.

Another method employs two sensors in a pitch-catch configuration where one sensor transmits an acoustic pulse and the other sensor acts as a receiver [2]. Authors' tests utilized a machined slot as a simulated crack and have demonstrated a reduction in received signal amplitude when the simulated crack was perpendicular to the path of the propagating wave. Expansion of this work also showed reduced signal amplitude caused by the presence of the simulated crack underneath the transmitter. Both of these experiments only used amplitude characteristics for a simulated crack. It was later demonstrated that a loose bolt in a joint could be detected using both amplitude and phase characteristics [8].

This paper explores further the ability of omni-directional pancake coil type MEAS in detecting structural damage in aluminum plates using linear and nonlinear techniques.

FATIGUE CRACK DETECTION USING MEAS

Sensor Description

In an effort to explore MEAS for various damage detection approaches two sensors with similar operational characteristics were selected. The selection was aimed at providing consistent experimental results as the same sensors were utilized as a transmitting and receiving pair for all reported pitch-catch experiments. Sensor C1 was used exclusively as a transmitter while C2 was used exclusively as a receiver. Table 1 – Table 3 give the sensor specifications. Also included are the specifications for sensor C8 which was used for the thickness resonance tests discussed later. As initial MEAS prototypes [2], these sensors were fabricated with steel housings providing both EMI shielding and a robust operation. Figure 1 shows a cross-sectional view of these sensors.

Table 1: Sensor Housing Specifications

Sensor	Diameter	Thickness
C1	1.000	0.400
C2	1.000	0.385
C8	1.000	0.982

Table 2: Sensor Magnet Specifications

Diameter	Thickness	Material
0.75	0.125	N52

Table 3: Sensor Coil Specifications

Sensor	Gage	ID	OD	Layers	Turns
C1	30	0.203	0.738	9	219
C2	30	0.219	0.762	9	222
C8	30	0.25	0.75	4	91

Figure 1 Cross-section of MEAS used in this study.

Experimental Setup and Test Procedures

A SHM experiment on detection of fatigue cracks using MEAS was conducted using thin plate aluminum specimens each featuring a machined slot in the center. The slot of 4cm long and 1.5mm wide was necessary to initiate fatigue cracks in one of the plates subjected to fatigue load. The undamaged (not subjected to fatigue) plate with a slot was used as a baseline to compare the results obtained from the fatigued specimen. Each plate measured 61cm x 61cm x 1mm. The fatigued plate was subjected to cyclic loading until a visible fatigue crack extending 5mm was present at the edge of the slot. Three sensor locations were chosen for each plate as shown in Figure 2. These locations were selected to provide maximum distance between sensors while remaining far enough away from the edges of the plate so that reflections would not interfere with the desired measurements. Sensor location 3 was chosen such that the elastic guided wave would pass directly through the fatigued crack located adjacent to the machined slot.

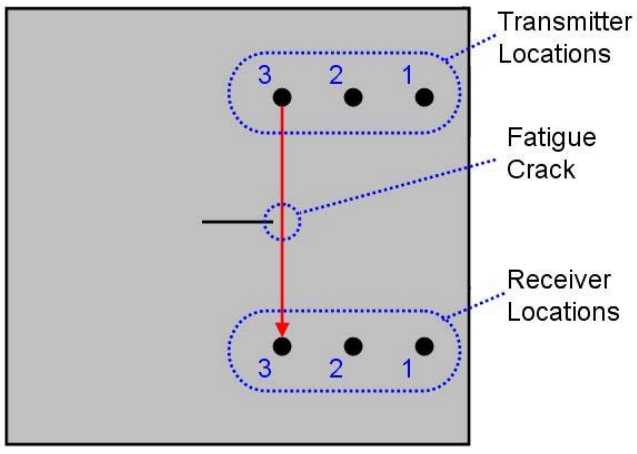

Figure 2 Test Setup showing sensor and fatigue crack locations.

Figure 3 shows the instrumentation setup for detection of fatigue cracks. A Ritec RAM-5000 high voltage measurement system was used to excite the transmitting MEAS [9]. An RF pulse was generated using the RAM's built in circuitry which then passed through a 50Ω high power terminator to improve signal generation. The pulse from the receiving MEAS was amplified by the RAM's internal amplifier. In addition to the high and low pass filters internal to the Ritec receiving amplifier a 100 Hz to 1 MHz Butterworth filter implemented in Labview was used in conjunction with signal averaging to reduce noise in the received signals. A NI PXI-5142 100MS/s high speed digitizer was used to digitize the transmitted and received signals which were made available for analysis using a PXIe 8360 MXI interface controller. Signals were then processed in LabVIEW and analyzed in Matlab.

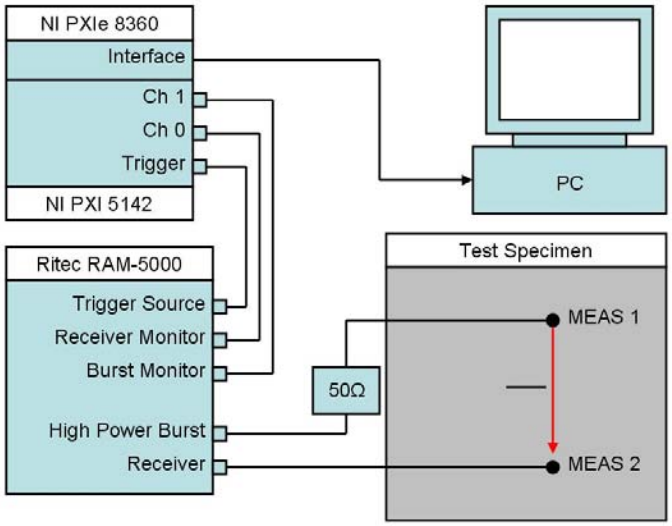

Figure 3 Instrumentation setup for detection of fatigue cracks.

During the fatigue damage detection experiment the MEAS was excited using a 300 kHz tone burst of varying duration. 300 kHz was determined experimentally to be an optimum frequency for exciting the S_0 wave mode with this test setup. Since two different plates were considered in these experiments, it became necessary to accurately position the MEAS relative to the machined slot. Sensor locations were carefully measured to ensure that they were as close to identical as possible for both of the plates. In addition, a wooden fixture designed by Tim Barnes [4] was used for sensor placement to ensure the distance between transducers remained the same, see Figure 4 for details.

Figure 4 Wooden fixture for placement of sensors.

At each sensor location (Figure 2) on both plates three measurements were taken using a 3 cycle, 8 cycle, and 35 cycle tone burst. For these measurements 4096 samples were averaged in order to reduce noise. After completing measurements, statistical variation of data was investigated in order to estimate the effects of sensor positioning errors. This was done by placing the sensors in one sensor location and taking a measurement using an 8 cycle tone burst with 256 samples being averaged. The sensors were then removed and placed in the same location for an additional measurement. Nine measurements were taken in this manner for each sensor location on both plates, so that tests yielded ten total measurements.

Fatigue Damage Manifestation in Signal Amplitude and Phase

The first methodology employed to detect fatigue damage examines the effect of the fatigue crack on amplitude and phase characteristics. It has been theorized that as the elastic wave propagates through the fatigued crack region, energy is redirected due to scattering resulting in a reduction of amplitude in the received pulse [1]. Therefore, the measured amplitude of a signal propagating in the fatigued plate should be less than the non-fatigued plate. In addition to amplitude reduction, local differences of elastic modulus between material inside and outside of the fatigue cracked region result in a phase change measured in the received pulse. This should result in a phase shift between the received signals from the fatigued plate and the non-fatigued plate.

Figure 5 shows the first pulse recorded by the receiver at location 3; which is the elastic S_0 wave mode. Other pulses arriving later are due to reflections resulting from plate geometry. This first pulse, however, should contain the effects of the fatigue crack region. An amplitude and phase change can be clearly seen when comparing the signals from the fatigued and non-fatigued specimens. The amplitude reduction is approximately 14% and the phase lag is approximately 28for this measurement.

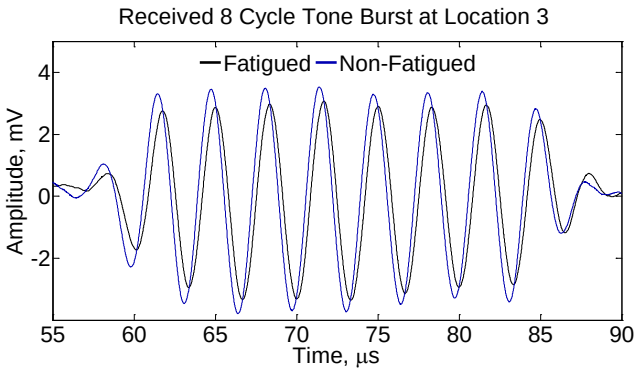

Figure 5 Received pulse showing a reduction in amplitude and change in phase between fatigued and non-fatigued specimens.

To investigate data variability caused by the experimental setup, a statistical analysis of the amplitude and phase change due to sensor positioning errors was performed. Figure 6 shows the 12 zero crossing points that were used for the statistical comparison. The average phase shift between the non-fatigued and fatigued specimen using 10 measurements was 32.6˚ with a standard deviation of 3.9˚. Figure 6 also shows the 10 signal peaks selected for the statistical comparison of amplitudes. Peak to peak amplitudes were used and the average reduction in amplitude for the fatigued specimen was 15.5% with a 3.4% standard deviation.

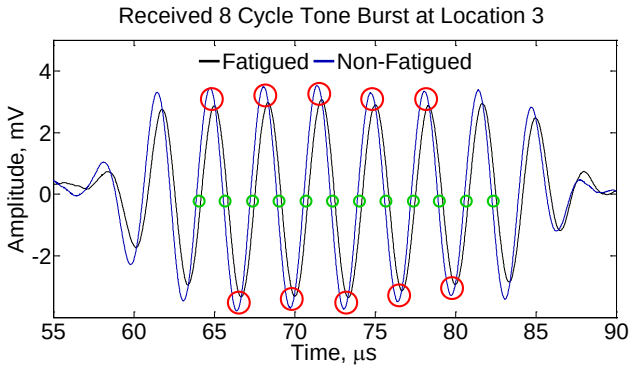

Figure 6 Green circles indicate location of zero-crossings used in the statistical analysis to calculate phase change. Red circles indicate amplitude peaks used in the statistical analysis to calculate the reduction in amplitude.

The collected data indicates that phase and amplitude changes between the fatigued and undamaged specimens can be easily measured with MEAS. Data from locations 1 and 2 were also analyzed using the same techniques used for location 3. Table 4 and Table 5 show the phase and amplitude differences between the fatigued and undamaged specimens at all three locations. The phase difference between locations on either undamaged or fatigued plates was insignificant.

Table 4: Phase difference (in degrees) between fatigued and intact specimens measured at indicated locations.

Location	1	2	3
Mean	32.2	32.5	32.6
Standard Deviation	4.6	3.6	3.9

Table 5: Percent amplitude reduction between fatigued and intact specimens at indicated locations

Location	1	2	3
Mean	3.0	4.5	15.5
Standard Deviation	3.8	2.5	3.4

In order to compare the data for the phase and amplitude a one way Analysis of Variance (ANOVA) was performed to compare samples. Table 6 shows the results of the ANOVA. The low percentages show that with 100% confidence the amplitude at location 3 is different than at locations 1 and 2. This confirms expectations that when the elastic wave is transmitted directly through the fatigue crack its amplitude is reduced. The comparison between locations 1 and 2 shows there is even a measureable difference between the amplitude at those locations. Results demonstrate that even a small amount of reduction in amplitude can be measured as the acoustic pulse' path is farther from the fatigue crack. The phase at locations 2 and 3 are identical with almost 90% confidence while location 1 is identical to location 2 and 3 with at least 48% confidence. The conclusion is that the phase at all three locations is not significantly different. This indicates that the phase shift measured between plates is not caused by the presence of the fatigue crack.

Table 6: Probability that phase and amplitude are the same

Locations	Amplitude	Phase
1 & 2	2.1%	53.7%
1 & 3	0%	47.9%
2 & 3	0%	89.7%

Factors that may cause the uniform phase shift could include preferable grain orientation, variability among plate material, or residual stresses due to the fatigue process. Under visual inspection, the plates revealed grain directions perpendicular to the machined slot, or parallel to the acoustic wave propagations path on both plates. In order to test for variability among plates an additional plate without a machined slot was used for a validation measurement. The sensors were randomly located on the plate parallel to the grain lines similar to the locations on the fatigued and non-fatigued plates. One sample was collected using the same setup used on the other plates. Figure 7 shows a comparison between the data from the fatigued, non-fatigued, and the extra plate. The extra plate data appears to be consistent with the non-fatigued plate data. It seems most likely that the phase shift in the fatigued plate is associated with residual stresses resulting from the fatigue process. Further testing is needed to confirm this hypothesis.

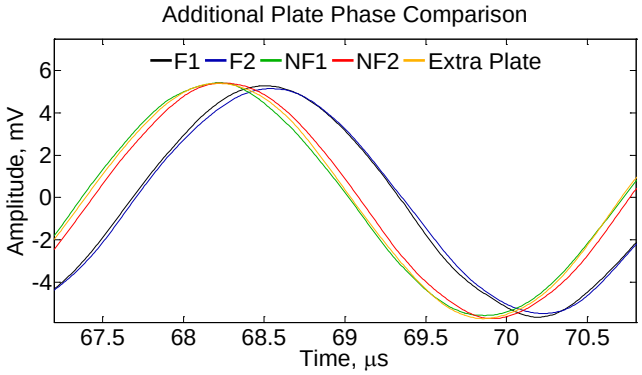

Figure 7 Phase shift comparison between the fatigued plate at locations 1 and 2 (F1 and F2) and the non-fatigued plate at locations 1 and 2 (NF1 and NF2) as well a measurement on an extra plate.

Additional investigations were conducted using ultrasonic pulses of different lengths. Examination of the phase and amplitude of the propagated 3 cycle pulse revealed trends similar to those previously observed in the records of 8 cycle pulse. Table 7 illustrates the phase and amplitude changes in the short pulse data. In contrast, examination of the 35 cycle pulse reveals unusual and sporadic results. It is suggested that such a behavior is caused by multiple reflections overlapping the directly transmitted pulse. Figure 8 and Figure 9 show examples of the short and long pulses.

Table 7 Phase difference and amplitude reduction between fatigued and intact specimens measured at indicated locations using a 3 cycle pulse.

Location	1	2	3
Phase Shift (Degrees)	31.5	29.6	32.4
Amplitude Reduction (%)	0.1	6.1	13.7

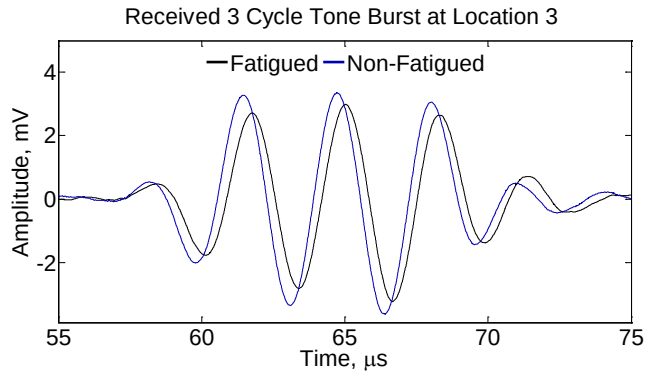

Figure 8 Short 3 cycle pulses from location 3

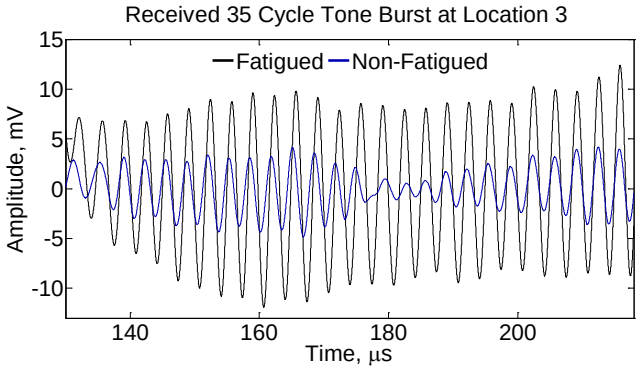

Figure 9 Long 35 cycle pulses from location 3

Analysis - Nonlinear Damage Detection

Material and structural damage induces nonlinearity of fundamental properties that may be probed by an ultrasonic signal. As an acoustic wave propagates through structural material, its waveform is affected by local material variations and manifests changes from its original sinusoidal pulse. Distortions of a sinusoidal component are typically reflected as additional harmonics in the spectrum of the measured signal [10]. Hence, our first method of nonlinear damage detection used Fourier frequency analysis to detect the presence of higher order harmonics. Figure 10 shows the expected results of the Fourier analysis for a perfectly linear and nonlinear specimen.

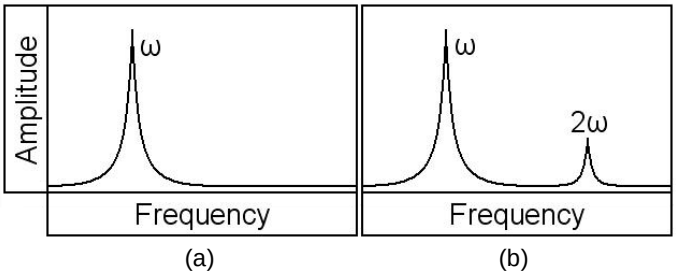

Figure 10 (a) Linear harmonic signal containing one frequency component. (b) Nonlinear harmonic signal showing additional higher order harmonic.

Because the Fourier transform theoretically implies consideration of infinite waveform, a continuous wave excitation would be ideal for this type of analysis. However, due to the limitations of the Ritec RAM-5000, a long tone burst of 35 cycles was used instead. The disadvantage of this approach is that due to geometry of the specimen, the directly transmitted S_0 mode is partially covered by the electromagnetic (EM) interference from the transmitting MEAS. In order to avoid influence of EM interference, the Fourier analysis was performed on the data recorded after the EM interference ceased. Figure 11 shows the resultant data and indicates that the second harmonic expected at 600 kHz is not visible. It appears that the 2nd harmonic is below the noise floor for this analysis and can not be used to infer information on material nonlinearity. The nonlinear fatigue damage is localized around the crack initiation slot and apparently contributes very little to a long pulse mostly travelling through intact material and containing additional reflection from plate boundaries.

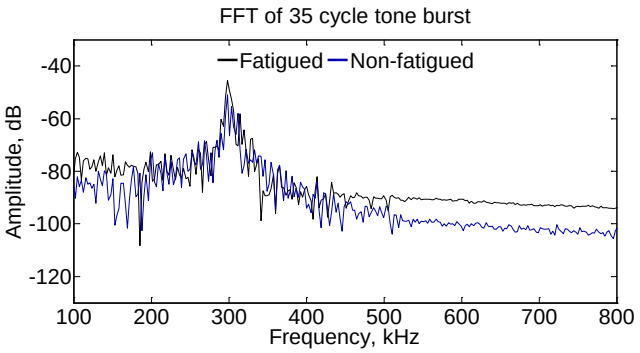

Figure 11 Frequency spectrum of 35 cycles signals measured on fatigued and non-fatigued specimens.

Instantaneous Phase

Another method considered for nonlinear damage detection explores the instantaneous phase of the acoustic signal. This technique requires defining an analytical signal:

$$z(t) = x_r(t) + i \cdot x_i(t), \tag{1}$$

where components $x_r(t)$ and $x_i(t)$ are the real signal and its Hilbert transform respectively. The instantaneous amplitude is then defined as the magnitude of $x_r(t)$ and $x_i(t)$ while the instantaneous phase is the angle between them:

$$|z(t)| = \sqrt{(x_r(t))^2 + (x_i(t))^2} \tag{2}$$

$$\varphi(t) = \tan^{-1}[x_i(t)/x_r(t)] \tag{3}$$

The instantaneous phase method has been shown to be a good measure of phase, matching results of zero-crossing techniques while providing improved resolution of phase shifts [8]. Its use in fatigue damage detection was also reported in [11]. Equation 3 provides a discontinuous function between the interval of $-\pi < \varphi(t) < \pi$. To correct this, the instantaneous phase must be unwrapped, meaning adding increments of $\pm 2\pi$. Figure 12 shows an example of the instantaneous phase for a 3 cycle pulse at location 3. The phase shift for this sample is 32.7 when using the difference between the two curves at 65μs. This matches well with the previous data calculated using zero-crossing points.

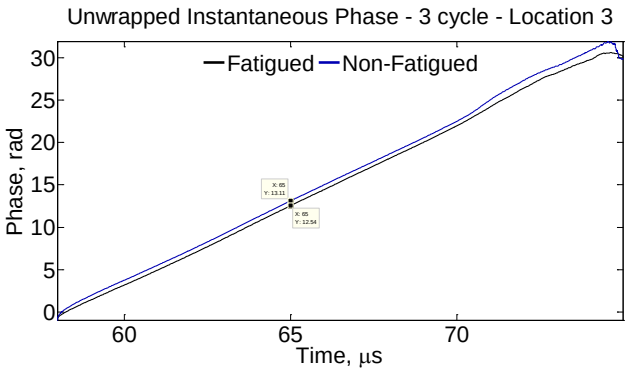

Figure 12 Instantaneous phase for a short 3 cycle pulse at location 3.

A number of features can be considered while analyzing the instantaneous phase. First, the slope of the instantaneous phase, or its derivative instantaneous frequency, should be constant for perfectly linear signals in a non-dispersive medium. An oscillatory motion in the frequency would indicate a nonlinear behavior. In addition, if the instantaneous frequency was not linear but curved it would show evidence of dispersion, see Figure 13. The hypothesis is that the signal passing through the fatigued crack would show a higher level of oscillation in the frequency and/or a higher level of dispersion than for the non-fatigued sample.

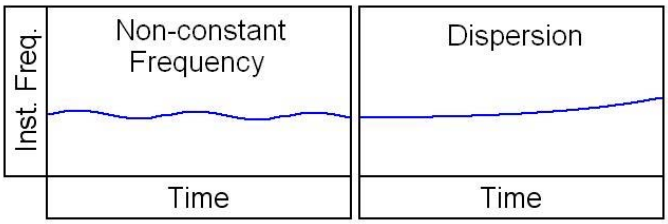

Figure 13 Observable effects using instantaneous frequency.

In order to approximate the instantaneous frequency, the instantaneous phase of an ideal sine wave was generated in Matlab and the instantaneous phase of the recorded signal was subtracted from the ideal instantaneous phase. Figure 14 shows the phase difference for a 3 cycle and 8 cycle tone burst. The shorter duration signal shows little distinction between the fatigued and non-fatigued specimens. The longer of the two signals shows a possible higher magnitude oscillation in the frequency. It should be mentioned that such oscillations may be generated by a constant zero frequency component in the signal and, to avoid misinterpretation, all signals were de-trended with a linear function before calculating instantaneous phase. After this procedure, the collected signals approximately satisfied the condition of zero mean and were admissible to the Hilbert transform.

Figure 14b illustrates deviation of instantaneous phase in the signals collected from fatigued and non-fatigues specimens. Higher magnitude of instantaneous phase oscillation was observed in the signal corresponding to fatigues specimen. A closer inspection of the central portion of the waveform (Figure 15a) shows a clearer difference between the signals.

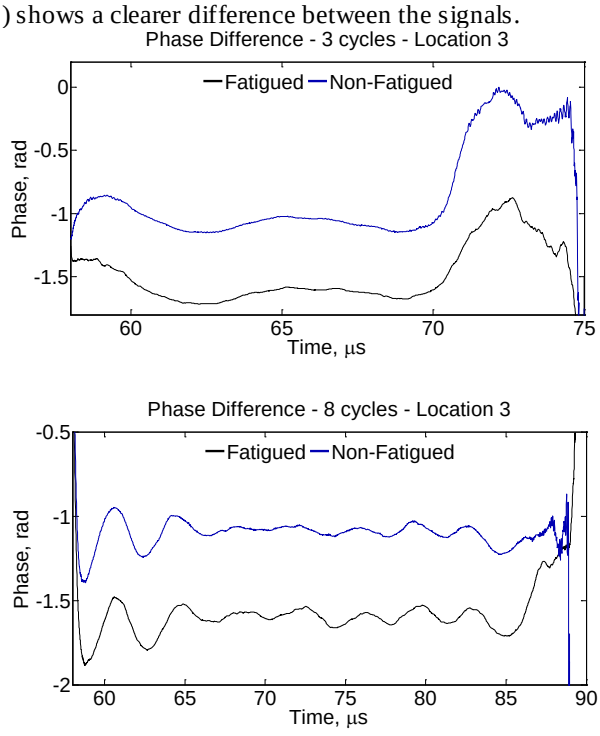

Figure 14 (a) Instantaneous phase deviation for 3 cycle tone burst. (b) Instantaneous phase deviation for 8 cycle tone burst.

In order to verify the cause of the higher amplitude instantaneous phase oscillation, a drive signal shifted by 180 was used to compare results and the same analysis was performed on data from location 3. Figure 15b shows the results obtained for the signal shifted by ˚.180 The phase difference does not seem to show the same trend when the drive signal is inverted. This raises questions regarding the fatigue contribution in the nonlinear signal depicted in Figure 15a. Figure 16 and Figure 17 depict results of the analysis for signals collected from location 1 and 2. The phase deviation of these signals does not show significant difference between fatigued and non-fatigued plates. Substantial dispersion was not noticed in data records from all three locations.

The instantaneous amplitude of an 8 cycle signal collected from both fatigued and non-fatigued specimens in location 3, shown in Figure 18, shows the signal delay (i.e. phase shift) as well as the amplitude reduction discussed in the previous section of the paper. Variation of amplitude versus time is more significant in fatigued data, but the difference is rather small. In general, amplitude reduction consistently indicates the presence of a fatigue crack. This feature may be supplemented with instantaneous phase deviation, which however was not a stable indicator of fatigue damage and its use in damage detection needs further clarification.

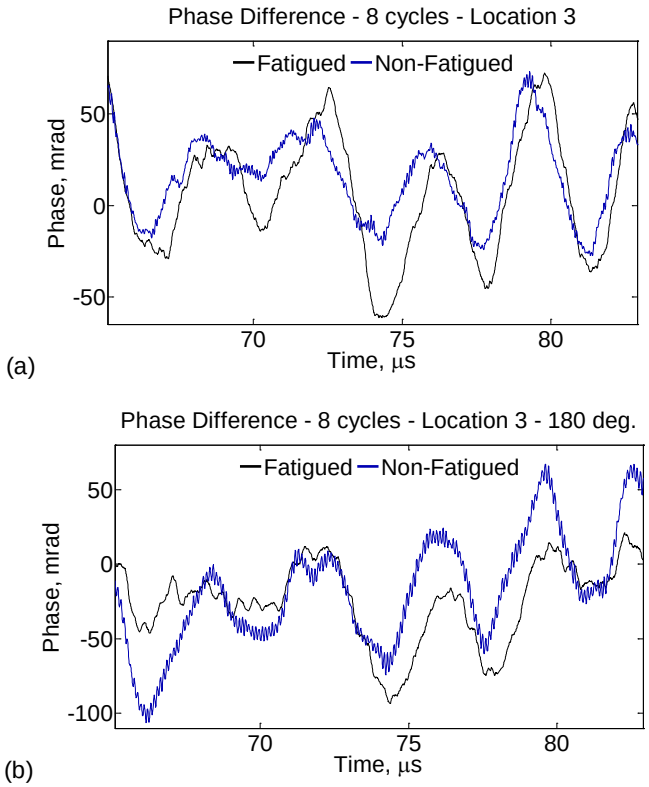

Figure 15 Close observation of phase oscillation in 8 cycle tone burst at location 3 with (a) 0 ˚ and (b) 180˚ offset drive signal.

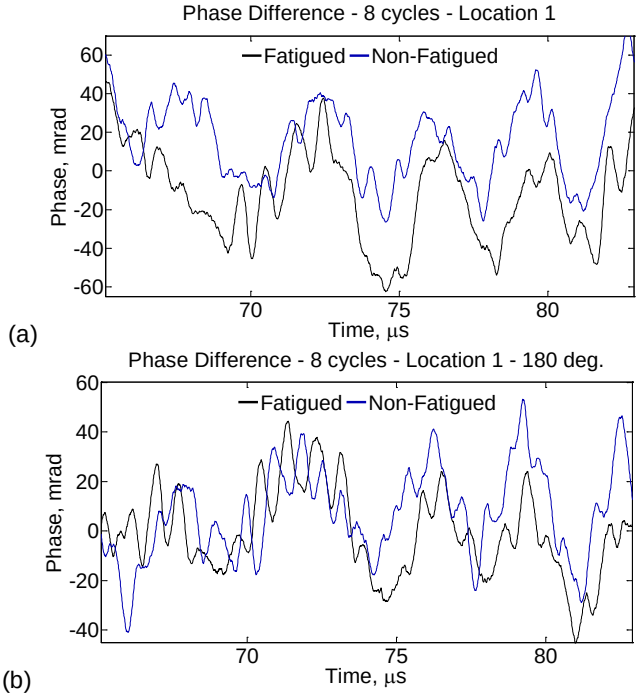

Figure 16 Close observation of phase oscillation in 8 cycle tone burst at location 1 with (a) 0 ˚ and (b) 180˚ offset drive signal.

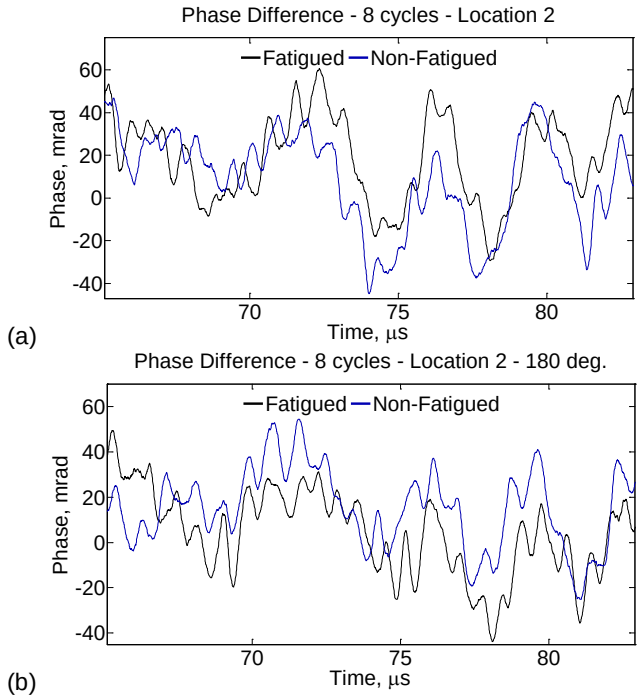

Figure 17 Close observation of phase oscillation in 8 cycle tone burst at location 2 with (a) 0 ˚ and (b)180˚ offset drive signal.

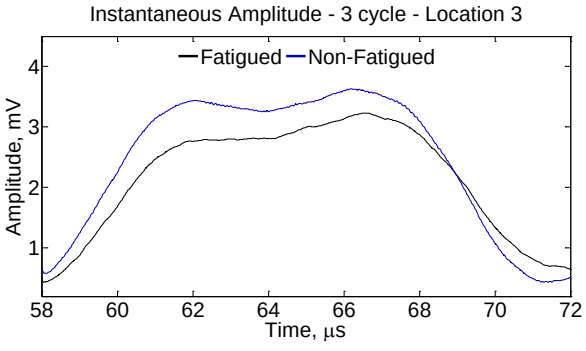

(a)

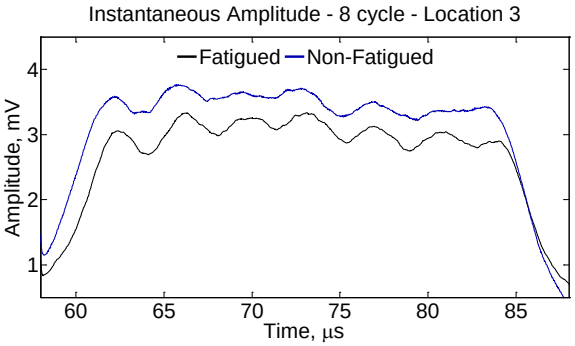

(b)

Figure 18 Instantaneous amplitude measured at locations 3 using (a) 3 cycle tone burst and (b) 8 cycle tone burst.

Thickness Resonance Tests

In addition to wave propagation experiments aimed at detection of structural damage in the MEAS far field, spectral measurements were conducted to evaluate sensor damage detection capabilities in the near field (in close proximity) of the sensor. This approach explored thickness resonance of the fatigued plate in locations next to and far away from a crack as illustrated in Figure 19. The presence of damage was evaluated by considering the distribution of resonances in the plate's frequency response.

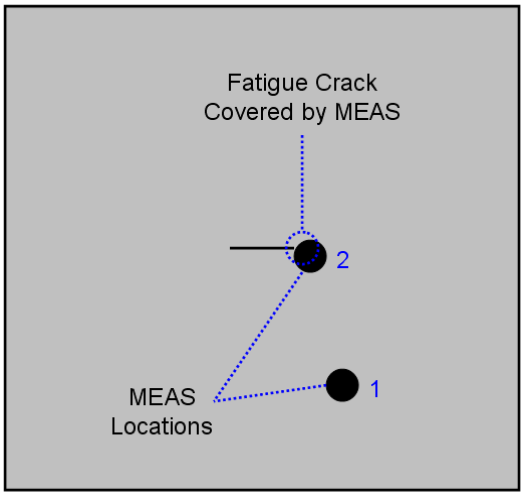

Figure 19 MEAS locations considered in thickness resonance tests.

The Ritec RAM was used to perform a resonance test using the equipment's built in frequency sweep mode. This allowed the MEAS to be excited with much longer bursts (200μs) and the frequency of each burst was varied incrementally to cover the desired frequency range. The two sensors were located on opposing sides of the plate directly above and below the other. After the burst was transmitted, a ring-down effect in the thickness volume was considered and data in the ring-down decaying portion of the waveform was analyzed. An integration window covering the ring-down region of the waveform was utilized to capture the magnitude of vibration at the fundamental frequency of vibration. Repeating a measurement process at each frequency, yielded the frequency responses illustrated in Figure 20.

In the thickness resonance measurements, sensor C8 was used as the transmitter and C1 as the receiver. A 200μs tone burst was transmitted and swept from 1-7 MHz in increments of 2 kHz. The integration window was 500μs long and began 150μs after transmission (excitation signal) ended. These parameters were determined experimentally to yield best results.

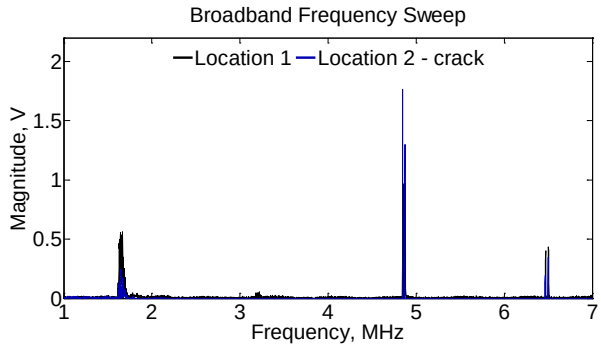

(a)

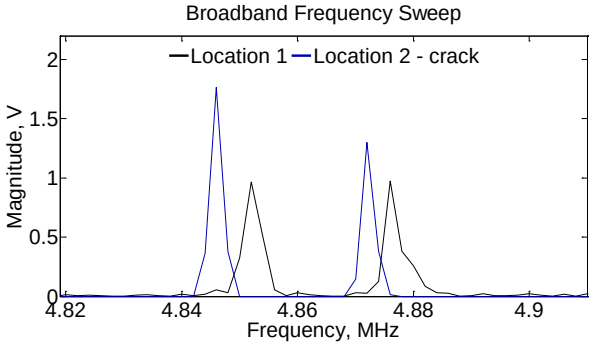

(b)

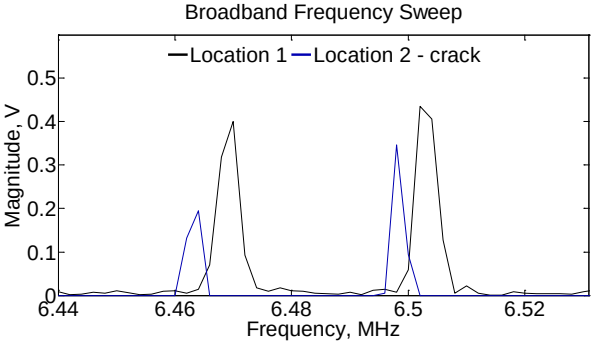

(c)

Figure 20 Results of thickness resonance tests.

Figure 20 shows a peak at 1.65 MHz as well as a double peak around both 4.86 MHz and 6.48 MHz. The double peak feature results from the capability of MEAS, in their current configuration, to excite shear waves of orthogonal polarization. Hence, each resonance peak indicates the particular orientation of the shear wave responsible for thickness resonance. The downward frequency shift in the location next to the crack was observed for the peaks located at 4.86 and 6.48 MHz. This may indicate the deterioration of material as the region becomes more compliant. However, another and even more interesting aspect of shear wave thickness resonance is the wider space between resonances for the fatigued plate than for the non-fatigued plate. The effect is known as a birefringence [12] and indicates residual stress in the region adjacent to crack. It is suggested that both features may be used for damage detection in the MEAS near field.

CONCLUSION

The paper discussed opportunities of using MEAS for active damage detection in aluminum alloy. Two approaches were utilized: elastic wave propagation and thickness resonance measurements. The first approach is recommended for damage detection in the MEAS far field while the second approach could be effective in detection of damage in the near field or underneath the sensor.

Elastic wave propagation characteristics in fatigued and non-fatigued plates differed in the phase of the propagating wave. Particularly there was a 32.6° phase difference between signals in the fatigued and non-fatigued plates. Measurements in different locations revealed that the fatigue crack may be reliably detected by analyzing amplitude changes in the signal. Instantaneous phase characteristics are also promising, but lack stability. Instantaneous phase needs to be explored in further investigations.

Thickness resonance tests revealed the capability of MEAS in measuring shear wave resonances and the birefringence effect. Resonances above 2MHz measured at the location of the fatigue crack have shown a noticeable downward frequency shift. The first peak at 1.65MHz did not show a substantial shift of the resonance peak. Birefringence can be clearly observed in Figures 20b and 20c. Wider spacing between peaks in the fatigue specimen indicates the presence of residual stress, which can be utilized as a structural diagnostic feature.

ACKNOWLEDGEMENT

Authors would like to acknowledge sponsorship of Air Force Office of Scientific Research (AFOSR) through contract FA9550-08-1-0128 and Federal Aviation Administration (FAA) support through COE for Commercial Space Transportation.

REFERENCES

[1] Giurgiutiu, V. (2007) *Structural Health Monitoring: with Piezoelectric Wafer Active Sensors*, Academic Press.

[2] Barnes, T., Kukhalashvili, D., Zagrai, A., (2010) "Magneto Elastic Active Sensors for Structural Health Monitoring using Magneto-Mechanical Impedance and Elastic Wave Propagation," *SPIE's 17th Annual International Symposium on Smart Structures and Materials and 15h Annual International Symposium on NDE for Health Monitoring and Diagnostics*, 7-11 March 2010, San Diego, CA, Vol. 7650, pp. 76501L.

[3] Banik, N.C. and Overhauser, A.W., (1977) "Electromagnetic Generation of Ultrasound in Metals," *Physical Review B*, Vol. 16, N. 8, pp. 3379-3388.

[4] Timothy Barnes (2010) *Development And Application of Magneto-Elastic Active Sensors for Structural Health Monitoring*, MS Thesis, New Mexico Institute of Mining and Technology.

[5] Grubin, H. L. (1970) "Direct Electromagnetic Generation of Compressional Waves in Metals in Static Magnetic Fields," IEEE Transactions on Sonics and Ultrasonics, Vol. SU-17, No. 4, October 1970.

[6] Aliouane, S., Hassam, M., Badidi-Bouda, A., and Benchaala, A. (2000) "Electromagnetic Acoustic Transducers (EMATs) Design Evaluation of their Performances," Proceedings of the 15th Wolrd Conference on Nondestructive Testing, October 2000

[7] Zagrai, A., Cakan, H., (2008) "Damage Diagnostics of Metallic Structures using Magneto-Mechanical Impedance Technique," Proceedings of SPIE, Vol. 6935, pp.6935-18.

[8] Murray, A., Zagrai, A., Conrad, D. (2011) "Diagnosis of Space Structures Using Embedded Sensors and Elastic Waves," Proceedings of SPIE's Symposium on Smart Structures and Materials and Non-Destructive Evaluation for Health Monitoring and Diagnostics, Vol. 7984, pp. 79840N.

[9] SNAP Operation Manual (2007) Ritec, Inc.

[10] Cantrell, J.H., Yost, W.T. (2001) "Nonlinear Ultrasonic Characterization of Fatigue Microstructures" International Journal of Fatigue, n 23, pp. S487-S490.

[11] Stolze, F., Staszewski, W.J., Manson, G and Worden, K. (2009) "An Investigation into the Instantaneous Phase of Guided Ultrasonic Waves in a Multi-Riveted Strap Joint Aluminum Panel," *Proceedings of the 7th International Workshop on Structural Health Monitoring*. September 9-11, 2009, Stanford, Ca.

[12] Hirao, M. and Ogi, H. (2003) *EMATS for Science and Industry – Noncontact Ultrasonic Measurements*, Kluwer Academic Publishers.